INORGANIC CHEMISTRY
FRONTIERS

RESEARCH ARTICLE

View Article Online
View Journal | View Issue

Cite this: *Inorg. Chem. Front.*, 2022, **9**, 4913

A spider hanging inside a carbon cage: off-center shift and pyramidalization of Sc_3N clusters inside C_{84} and C_{86} fullerene cages†

Ze Fu, ‡ Min Guo,‡ Yang-Rong Yao,‡ Qingyu Meng, Yingjing Yan, Qin Wang, Yi Shen and Ning Chen *

Metal nitride cluster fullerenes (NCFs) are the most intensively studied endohedral fullerenes due to their exceptional structural variety. It is commonly understood that in NCFs, small clusters such as Sc_3N favor C_{82} and smaller cages, while large clusters (*e.g.*, Tb_3N and Gd_3N) favor C_{84} and larger cages. Endohedral structures with small nitride clusters encaged inside large carbon cages (*e.g.*, C_{84} and C_{86}), although theoretically probed, have never been experimentally obtained. Herein, we report two novel NCFs, $Sc_3N@C_s(51365)$-C_{84} and $Sc_3N@D_3(19)$-C_{86}, which have been successfully synthesized and characterized using MALDI-TOF mass spectrometry, X-ray single-crystal diffraction and UV–vis–NIR spectroscopy. Crystallographic analysis shows that, while in most previously reported cluster fullerenes, clusters tend to take a central position inside fullerene cages, in these two structures, the Sc_3N clusters are shifted to one side of the cage and unexpectedly pyramidalized inside the large cages of C_{84} and C_{86}, which resembles a spider hanging inside a carbon cage. These observations, together with the stretched Sc–N bonds, suggest that the M_3N cluster can self-adjust not only its configuration but also its position relative to fullerenes to optimize the metal–cage distances as well as cluster–cage interactions, thus promoting the stability of endohedral structures. This work provides new insight into the interaction mechanisms between the clusters and carbon cages of endohedral fullerenes.

Received 22nd June 2022,
Accepted 1st August 2022

DOI: 10.1039/d2qi01318e

rsc.li/frontiers-inorganic

Introduction

Endohedral metallofullerenes (EMFs) feature unique host–guest molecular structures in which metal ions or metallic clusters are encapsulated in variable carbon cages. Complex metal–cage interactions are formed between endohedral moieties and fullerene cages, which are essential for the stability of these endohedral fullerene compounds.[1–3] Endohedral fullerenes have shown great potential in the application of biomedicine, catalysis and molecular electronic devices due to their unique molecular and electronic structures.[4–7]

Among the EMFs, cluster fullerenes (CFs) are the largest family, with variable clusters encapsulated inside fullerenes. Since the discovery of $Sc_3N@C_{80}$ in 1999, in the past two decades, this family has been largely expanded and extensively studied, including metal nitride cluster fullerenes (NCFs), metal carbide cluster fullerenes (CCFs) and metal cyanide cluster fullerenes (CYCFs).[8,9] One of the interesting studies for CFs is the cluster configuration variations in cluster fullerenes, which is important for understanding the interactions between clusters and carbon cages.[9] Previous studies found that clusters with flexible configurations, such as M_2C_2, M_2O and MCN, can adjust their configurations inside the confined space of fullerene cages to achieve optimized metal–cage interactions, which contributes to the stabilization of host–guest molecular structures.[10–13] Factors such as different carbon cage isomers, the size of the carbon cage and the metal ionic radii of encapsulated clusters can all lead to changes in the cluster configuration.[14–18] For instance, as the size of the carbon cage decreases, M_2C_2 clusters change from a nearly linear stretched geometry to a constrained "butterfly" structure, whereas MCN clusters change from a nearly linear shape to a triangular configuration.[13,19,20] Moreover, in non-IPR (isolated pentagon rule) carbon cages, clusters can be deformed to obtain stronger interactions with the carbon cage due to the high local strain of the heptagon or fused pentagons, thus stabilizing these carbon cages.[21–27] Overall, these flexible encaged clusters can self-adjust their size and shape to achieve optimal

College of Chemistry, Chemical Engineering and Materials Science, and State Key Laboratory of Radiation Medicine and Protection, Soochow University, Suzhou, Jiangsu 215123, P. R. China. E-mail: chenning@suda.edu.cn

†Electronic supplementary information (ESI) available. CCDC 2178354 and 2178355. For ESI and crystallographic data in CIF or another electronic format see DOI: https://doi.org/10.1039/d2qi01318e

‡These authors contributed equally to this work.

metal–cage interactions, which is essential for the stability of cluster fullerene compounds.

NCFs have been the most abundant and most intensively studied endohedral fullerenes in the past decade. Trimetallic nitride clusters have a relatively rigid configuration compared with M_2O, M_2C_2 and MCN clusters. Thus, due to their less flexible configurations, it has been well acknowledged that large nitride clusters tend to be encapsulated inside large carbon cages, while small clusters tend to be encapsulated in small carbon cages to maintain their planarity.[28] In addition, large-sized metal nitride clusters tend to be pyramidalized inside small carbon cages.[29–31] However, how small rigid clusters interact with large cages (*e.g.*, C_{84} and C_{86}) has never been experimentally observed and studied. Sc_3N is the smallest encapsulated cluster in NCFs, as the ionic radius of Sc (0.75 Å) is much smaller than those of other lanthanides, such as Er (0.89 Å), Tb (0.92 Å) and Gd (0.94 Å). Previous theoretical studies suggest that the Sc_3N cluster is off-center inside cages larger than C_{82}, whereas this displacement leads to a less effective cluster–cage interaction, which is likely unstable. Thus, $Sc_3N@C_{2n}$ cluster fullerenes with a cage size of C_{84} and larger are almost impossible to obtain.[32] As a result, whether small clusters such as Sc_3N, which has a relatively rigid configuration, can be stabilized inside large fullerene cages such as C_{84} and C_{86} has remained unknown to date.

Herein, we report the synthesis and isolation of two novel NCFs, $Sc_3N@C_s(51365)$-C_{84} and $Sc_3N@D_3(19)$-C_{86}, which were characterized by MALDI-TOF mass spectrometry, X-ray single-crystal diffraction, UV–vis–NIR spectroscopy and Fourier transform infrared spectroscopy. The detailed structural analysis demonstrates that the clusters show an off-center shift to one side of the cage and unexpected pyramidalization in both C_{84} and C_{86}.

Results and discussion

Synthesis and isolation of $Sc_3N@C_{2n}$ ($2n$ = 84 and 86)

Scandium-based endohedral fullerenes were synthesized using a modified Krätschmer–Huffman (direct-current) DC arc-discharge method. Graphite rods packed with Sc_2O_3/graphite powder (with a molar ratio of Sc/C = 1 : 15) were annealed and then vaporized in an arcing chamber under a 200 Torr helium and 4 Torr nitrogen atmosphere. The collected raw soot was extracted with carbon disulfide (CS_2) for 24 h. Multiple-stage high-performance liquid chromatography (HPLC) separation processes were employed to isolate and purify $Sc_3N@C_{84}$ and $Sc_3N@C_{86}$ (Fig. S1 and S2, ESI†). The purity of the isolated compounds was confirmed by the observation of single peaks using HPLC and high-resolution positive-ion-mode matrix-assisted laser desorption ionization time-of-flight (MALDI-TOF) mass spectrometry (Fig. S3† and Fig. 1). The mass spectra of purified $Sc_3N@C_{84}$ and $Sc_3N@C_{86}$ show single peaks at m/z = 1157.053 and 1180.970, respectively, which are similar to theoretical simulations. Furthermore, the isotopic distributions in the experiment were found to be quite similar to the theoretical prediction.

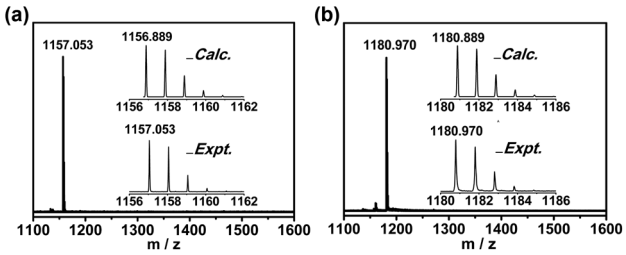

Fig. 1 Positive mode MALDI-TOF mass spectra of purified (a) $Sc_3N@C_{84}$ and (b) $Sc_3N@C_{86}$. Insets: experimental and theoretical isotopic distributions for (a) $Sc_3N@C_{84}$ and (b) $Sc_3N@C_{86}$.

Molecular structures of $Sc_3N@C_{84}$ and $Sc_3N@C_{86}$

$Sc_3N@C_{2n}$ ($2n$ = 84 and 86) was cocrystallized with Ni^{II}(OEP) (OEP = 2, 3, 7, 8, 12, 13, 17, and 18-octaethylporphyrin dianion) to obtain crystals suitable for X-ray measurements. The molecular structures of $Sc_3N@C_{84}$ and $Sc_3N@C_{86}$ were unambiguously determined using single-crystal X-ray diffraction analysis as $Sc_3N@C_s(51365)$-C_{84} and $Sc_3N@D_3(19)$-C_{86}, respectively. Fig. 2a and b shows the cocrystal structures formed by these

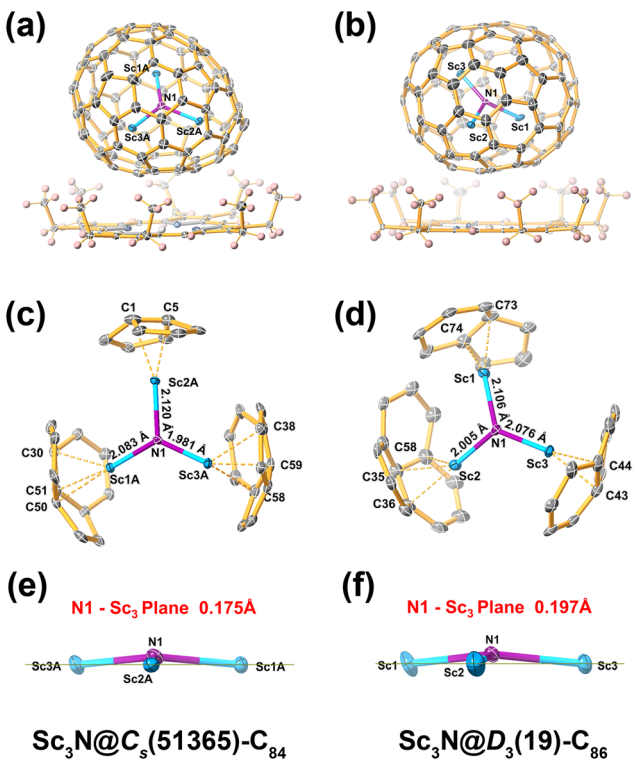

Fig. 2 Oak ridge thermal ellipsoid plot (ORTEP) drawings showing the relative orientations of NCFs and porphyrin moieties for (a) $Sc_3N@C_{84}$·Ni^{II}(OEP) and (b) $Sc_3N@C_{86}$·Ni^{II}(OEP) with 20% thermal ellipsoids. Only the major fullerene cage and the predominant cluster orientations are shown. For clarity, the solvent molecules and minor sites are omitted. A view of the relationship between the major metal nitride clusters and the closest cage portions in (c) $Sc_3N@C_s(51365)$-C_{84} and (d) $Sc_3N@D_3(19)$-C_{86}. A view of the Sc_3N portions at the major sites shows the out-of-plane displacements of the nitrogen atoms in (e) $Sc_3N@C_{84}$ and (f) $Sc_3N@C_{86}$.

NCFs with the Ni^{II}(OEP) moiety. The closest distances between the nickel atom and the carbon atoms on the cage were measured as 3.029 and 2.981 Å for $Sc_3N@C_s$(51365)-C_{84} and $Sc_3N@D_3$(19)-C_{86}, respectively, suggesting substantial π–π interactions between the fullerene cage and the porphyrin moiety.

Crystallographic analysis shows that the cocrystals crystallized in the triclinic space group of *P*1 for $Sc_3N@C_s$(51365)-C_{84} and the monoclinic space group of *C*2/*m* for $Sc_3N@D_3$(19)-C_{86}. The C_s(51365)-C_{84} carbon cage and the internal nitrogen atom are fully ordered, while the encapsulated metal atoms exhibit a slight disorder. For Sc1A, Sc2A and Sc3A, which constitute the major Sc_3N sites, the occupancy is 0.746(4). The minor Sc_3N sites comprise Sc1B, Sc2B, and Sc3B with an occupancy of 0.254(4) (Fig. S4a†). For $Sc_3N@D_3$(19)-C_{86}, the fullerene cage shows two orientations due to the crystallographic mirror of the *C*2/*m* space group. A complete fullerene cage with an occupancy of 0.5 is formed by combining one-half of one orientation and the mirror-related half of the other orientation. The scandium atoms have six crystallographic sites, with 0.313 occupancy for Sc in the major cluster (Sc1, Sc2 and Sc3) and 0.18 occupancy for Sc in the minor cluster (Sc4, Sc5 and Sc6). Moreover, six additional metal sites ($Sc1_m$, $Sc2_m$, $Sc3_m$, $Sc4_m$, $Sc5_m$ and $Sc6_m$) are generated *via* the crystallographic mirror plane (Fig. S4b†). Both of the major Sc_3N clusters in both C_{84} and C_{86} show a relatively high occupancy, which allows a more precise analysis of their configurations and their interactions with the fullerene cages.

Interaction between Sc_3N clusters and large carbon cages

Fig. 2c and d shows the relative positions of the major Sc_3N sites to the corresponding cage portions. In $Sc_3N@C_s$(51365)-C_{84}, one of the three Sc atoms is located under the conjunction of fused pentagons, and the other two Sc atoms are located below a [5,5,6] junction ([5] and [6] refer to pentagon and hexagon, respectively). The shortest average distances between the three Sc atoms and the carbon cage are 2.303(10) Å (Sc2A–C5 and Sc2A–C1), 2.276(8) Å (Sc1A–C51 and Sc1A–C30) and 2.306(8) Å (Sc3A–C59 and Sc3A–C38), respectively. Regarding $Sc_3N@D_3$(19)-C_{86}, Sc1 is located below a [5,6] junction with the shortest average metal–cage distance of 2.230(15) Å (Sc1–C74 and Sc1-C73). Sc2 and Sc3 are located under a [6,6] junction and a [6,6,6] junction with the shortest average metal–cage distances of 2.167(13) Å (Sc2–C58 and Sc2–C36) and 2.131(16) Å (Sc3–C44 and Sc3–C43), respectively. In general, these Sc–C distances are similar to the Sc–C distances between Sc_3N clusters and smaller cages, such as $Sc_3N@C_{2n}$ ($2n$ = 68, 78, 80, 82; for details please see Table 1).

The Sc–N distances of the Sc_3N cluster in the C_s(51365)-C_{84} cage are 2.083(6) Å for Sc1A–N, 2.120(6) Å for Sc2A–N, and 1.981(6) Å for Sc3A–N. The longer bond length of Sc2A–N can be well explained by the fused pentagons coordinated to Sc2A, which strongly interact with Sc2A and withdraw the electron density from the Sc–N unit, thus weakening the Sc–N bond interaction. Similar phenomena have been observed in other non-IPR nitride cluster fullerenes, such as $M_3N@C_2$(22010)-C_{78} (M = Gd, Tb and Ho),[24,25] $M_3N@C_s$(39663)-C_{82} (M = Gd and Sc),[26,27] and $M_3N@C_s$(51365)-C_{84} (M = Gd, Tb, Er, Tm, Lu and Sc).[33–36]

Unlike the non-IPR cage of C_s(51365)-C_{84}, there are no fused pentagons in the cage of D_3(19)-C_{86}. However, unexpectedly, one of the Sc–N bonds, Sc1–N, also has a longer distance of 2.106(7) Å, compared with 2.005(5) Å for Sc2–N and 2.076(6) Å for Sc3–N, suggesting that Sc1–N is stretched out to facilitate a closer metal–cage contact in IPR D_3(19)-C_{86}. Notably, the

Table 1 Selected interatomic distances and angles

	$Sc_3N@C_s$(51365)-C_{84}	$Sc_3N@D_3$(19)-C_{86}	$Sc_3N@D_3$(6140)-C_{68} [38,39]	$Sc_3N@D_{3h}$(5)-C_{78} [40]
Distance (Å)				
M1–N	2.083(6)	2.106(7)	2.022(3)	1.988(7)
M2–N	2.120(6)	2.005(5)	1.974(4)	1.983(15)
M3–N	1.982(6)	2.076(6)	1.961(4)	2.125(5)
Metal–C[a]				
M1–C	2.225(8)–2.602(8)	2.188(15)–2.632(17)	2.247(5)–2.387(5)	2.058(3)–2.443(3)
M2–C	2.276(10)–2.413(9)	2.146(13)–2.503(18)	2.222(5)–2.381(5)	2.024(16)–2.440(17)
M3–C	2.266(7)–2.661(9)	2.088(15)–2.612(12)	2.237(5)–2.380(5)	2.075(4)–2.440(5)
Angles (°)				
∑(M–N–M)	357.9	357.2	359.8	360.0
	$Sc_3N@D_{5h}$(6)-C_{80} [41]	$Sc_3N@I_h$(7)-C_{80} [8]	$Sc_3N@C_{2v}$(39718)-C_{82} [42]	$Sc_3N@C_s$(39663)-C_{82} [27]
Distance (Å)				
M1–N	2.014(2)	2.011(19)	2.007(4)	2.112(3)
M2–N	2.031(2)	1.966(12)	2.078(3)	2.052(4)
M3–N	2.041(2)	1.95(3)	2.078(3)	2.038(3)
Metal–C[a]				
M1–C	2.255(3)–2.512(3)	2.188(10)–2.508(13)	2.269(17)–2.607(23)	2.316(6)–2.444(6)
M2–C	2.269(3)–2.624(3)	2.148(10)–2.516(13)	2.190(17)–2.613(11)	2.272(6)–2.553(5)
M3–C	2.232(3)–2.537(3)	2.18(3)–2.43(3)	2.117(15)–2.452(11)	2.256(5)–2.578(6)
Angles (°)				
∑(M–N–M)	359.9	360.0	359.9	359.5

[a] Range of distances between the metal atom and the nearest six carbon atoms.

stretching of M–N bonds in $M_3N@D_3(19)$-C_{86} (M = Gd and Tb) has not been observed.[31,37] Thus, this stretched configuration of Sc_3N inside $D_3(19)$-C_{86} suggests that small encapsulated metallic clusters (Sc_3N) can adapt their configurations not only inside non-IPR fullerene cages, as generally acknowledged but also in larger IPR fullerene cages, such as C_{86}, to facilitate a closer interaction with the carbon atoms on fullerene cages, which is beneficial for the stabilization of the whole EMF molecule.

Pyramidalization of Sc_3N clusters inside large cages

Fig. 2e and f show the out-of-plane position of nitrogen atoms in the Sc_3N clusters inside $C_s(51365)$-C_{84} and $D_3(19)$-C_{86}, respectively. The Sc–N–Sc angles in the cages of $C_s(51365)$-C_{84} and $D_3(19)$-C_{86} are 357.9° and 357.2°, respectively, suggesting that the Sc_3N clusters do not adapt to a fully planar configuration. Moreover, the nitrogen atom is 0.175 Å out of the Sc_3 plane in $Sc_3N@C_s(51365)$-C_{84} and 0.197 Å out of the Sc_3 plane in $Sc_3N@D_3(19)$-C_{86}, indicating a slight pyramidalization of Sc_3N clusters. This observation is rather unexpected as Sc_3N is the smallest metallic nitride cluster in the NCF family and always adapts a planar configuration inside fullerene cages, ranging from C_{68} to C_{82}, as shown in Table 1 and Fig. 4 and S5†[8,27,38–42] In fact, to date, the pyramidalization of clusters has only been observed for large clusters, such as Y_3N and Gd_3N, encaged inside cages smaller than C_{82}. The main cause for this pyramidalization of metallic clusters is the forced squeezing of the large-sized clusters in the small carbon cages, such as $M_3N@I_h(7)$-C_{80} (M = Y, Gd and Tb).[29–31] A general expectation would be that small clusters would not suffer from the compression of the carbon cage and thus would easily adapt to a fully planar configuration. This result, however, validates that small clusters can also be pyramidalized in large cages. Thus, it suggests that the driving force for the pyramidalization of encapsulated clusters is not merely the compressing effect of the cage but, more generally, the self-adaptation of clusters, which facilitates an appropriate interaction between the metal ion and the carbon atoms on the cage.

Off-center shift of the Sc_3N clusters inside large cages

Fig. 3a shows the positions of clusters in the carbon cages of $M_3N@C_s(51365)$-C_{84} (M = Gd, Tb, Er, Tm, Lu and Sc).[33–36] It can be clearly observed that in the previously reported NCFs, such as $M_3N@C_s(51365)$-C_{84} (M = Gd, Tb, Er, Tm and Lu), the M_3N clusters are all located at the center of the fullerene carbon cages. In comparison, the Sc_3N cluster notably shifts from the center of the carbon cage to one side of the $C_s(51365)$-C_{84} cage. The same off-center location of the inner Sc_3N cluster is observed for $Sc_3N@D_3(19)$-C_{86}. For comparison, all of the larger clusters, such as Gd_3N and Tb_3N, are located at the center of the carbon cage, and the nitrogen atoms are located on the 3-fold axis of the $D_3(19)$-C_{86} cage (Fig. 3c).[31,37]

In addition, Fig. 3b shows the relative positions for the symmetry plane of the $C_s(51365)$-C_{84} cage (marked in red) and the planes of the metal nitride clusters (marked in green) in $M_3N@C_s(51365)$-C_{84} (M = Gd, Tb, Er, Tm, Lu and Sc).[33–36] It shows that inside C_{84} cages, the dihedral angles between the planes of clusters and the symmetry plane are in the range of 22.2°–26.7°, whereas the dihedral angle between the Sc_3N

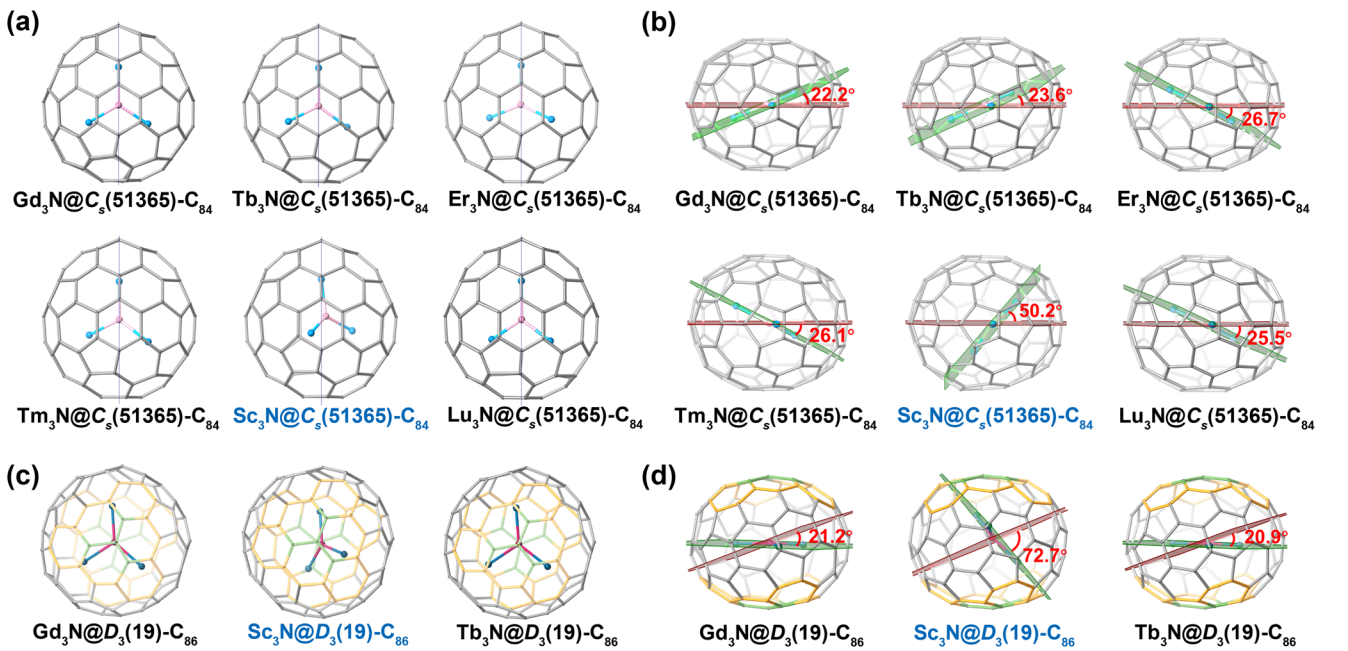

Fig. 3 (a) Molecular structures of $M_3N@C_s(51365)$-C_{84} (M = Gd, Tb, Er, Tm, Lu and Sc) showing the differences in metal nitride cluster positions. (b) A top view of $M_3N@C_s(51365)$-C_{84} (M = Gd, Tb, Er, Tm, Lu and Sc) with the planes of symmetry marked in red and the planes of the metal nitride clusters marked in green. (c) A view down the 3-fold axis of $M_3N@D_3(19)$-C_{86} (M = Gd, Tb and Sc) showing the differences in metal nitride cluster positions. (d) The planes that equally divide the lateral hexagons are marked in red, and the planes of the metal nitride clusters in $M_3N@D_3(19)$-C_{86} (M = Gd, Tb and Sc) are marked in green.

plane and the symmetry plane is 50.2°, suggesting its considerable shift from the center. An even greater off-center shift is observed for $Sc_3N@D_3(19)$-C_{86}. The dihedral angle in this case, formed by the plane that bisects the lateral hexagon (marked in red) and the plane in which the Sc_3N cluster is located (marked in green), notably increases to 72.7° in $Sc_3N@D_3(19)$-C_{86} (Fig. 3d). For $M_3N@D_3(19)$-C_{86} (M = Gd and Tb), in which the larger Gd_3N and Tb_3N clusters are located at the center of the cages, the corresponding dihedral angles are only in the range of 20.9–21.2°.[31,37]

On the other hand, Fig. 4 and Fig. S6† show that the distances between the Sc-triangle planes and the center of gravity of the carbon cages are in the range of 0.005–0.110 Å from C_{68} to C_{82}. However, the distances of $Sc_3N@C_{84}$ and $Sc_3N@C_{86}$ increase significantly to 0.473 Å and 0.504 Å, respectively, which also indicates the dramatic off-center shift of the Sc_3N clusters in the C_{84} and C_{86} carbon cages.[8,27,38–42]

Discussion

Previously, it was generally acknowledged that relatively small nitride clusters, such as Sc_3N, favor C_{80} and smaller cages; for large clusters such as Nd_3N, encapsulation into the C_{88} or larger cages is energetically preferred.[28] These theories have also been verified by many experimental results.[8,38–40,42–45] Interestingly, NCFs in which smaller clusters are encapsulated inside large cages, such as $Sc_3N@C_{2n}$ with cages larger than C_{82}, have never been observed before. On the other hand, theoretical calculations on NCFs predicted the off-center shift of the Sc_3N clusters in large carbon cages such as C_{84}, C_{88} and C_{96}.[28,32] Meanwhile, they also pointed out that this shift could result in a less effective cluster–cage interaction; thus, the Sc_3N-based NCFs with cage sizes of C_{84} and larger might not be very stable, which was consistent with the absence of experimental reports of these structures.[32] The above crystallographic analysis, however, validates the stabilization of $Sc_3N@C_{84}$ and $Sc_3N@C_{86}$. Moreover, it reveals the off-center shift and, surprisingly, the slight pyramidalization of the Sc_3N clusters in these large cages. These observations, together with the stretched Sc–N bonds, suggest that in large cages, due to the small size, the Sc_3N cluster favors an off-center location and attaches to one side of the carbon cage like a spider. In addition, it can also adjust its configuration to be slightly pyramidalized to further optimize the Sc–N distances and metal–cage interactions, ultimately forming stable host–guest molecular compounds.

UV–vis–NIR spectroscopic characterization

The purified samples of $Sc_3N@C_s(51365)$-C_{84} and $Sc_3N@D_3(19)$-C_{86} dissolved in carbon disulfide (CS_2) were characterized using UV–vis–NIR absorption spectroscopy, as shown in Fig. 5. The spectrum of $Sc_3N@C_s(51365)$-C_{84} shows two minor shoulder peaks (480 and 669 nm, respectively) with an onset at approximately 1350 nm, resulting in an optical band gap of 0.92 eV. The absorption spectrum is almost identical to the previously reported spectra of $M_3N@C_s(51365)$-C_{84} (M = Er, Lu, Gd, Tb and Tm),[33–36] suggesting that they have the same cage symmetries and charge transfer patterns. In the spectrum of $Sc_3N@D_3(19)$-C_{86}, two shoulder peaks at 496 and 691 nm are observed, which are similar to the absorption spectrum of $Tb_3N@D_3(19)$-C_{86},[31] indicating that they have the same isomeric structures. The absorption onset is measured at approximately 1400 nm, and the optical band gap is determined to be 0.88 eV. In addition, the optical band gaps of $Sc_3N@C_s(51365)$-C_{84} and $Sc_3N@D_3(19)$-C_{86} are smaller than those of the other reported members of the NCF family with the same carbon cages.[31,33–36] Such small optical band gaps of $Sc_3N@C_s(51365)$-C_{84} and $Sc_3N@D_3(19)$-C_{86} suggest that a further increase in the large carbon cage size is not favorable

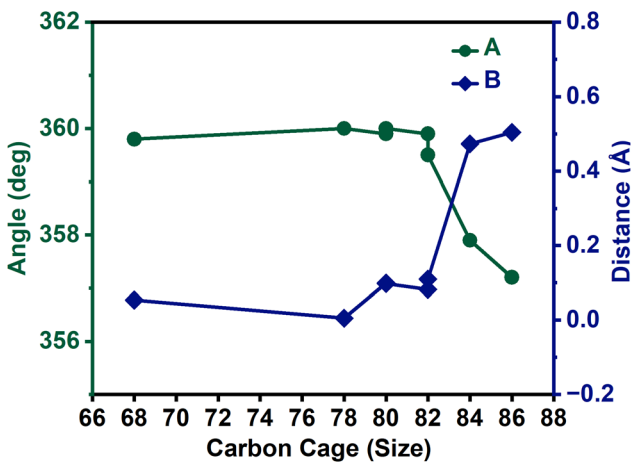

Fig. 4 The Sc–N–Sc angles (A, in degrees) and the distances between the Sc-triangle planes and the center of gravity of carbon cages (B, in angstroms) with respect to the sizes of carbon cages for $Sc_3N@C_{2n}$ ($2n$ = 68, 78, 80, 82, 84, and 86).

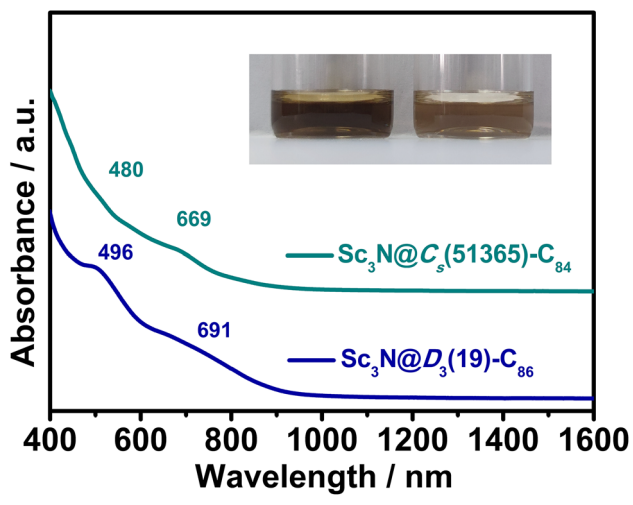

Fig. 5 UV–vis–NIR absorption spectra of $Sc_3N@C_s(51365)$-C_{84} and $Sc_3N@D_3(19)$-C_{86} in CS_2 solution. The inset shows a photograph of $Sc_3N@C_s(51365)$-C_{84}(left) and $Sc_3N@D_3(19)$-C_{86}(right) dissolved in CS_2. The curves are vertically shifted for ease of comparison.

for Sc_3N cluster fullerene formation, which is consistent with theoretical calculations.[32]

Conclusions

In summary, two novel nitride cluster fullerenes, $Sc_3N@C_{2n}$ ($2n$ = 84 and 86), have been successfully synthesized and characterized by MALDI-TOF mass spectrometry, single-crystal XRD and UV–vis–NIR spectroscopy. The molecular structures of the two NCFs were identified as $Sc_3N@C_s(51365)$-C_{84} and $Sc_3N@D_3(19)$-C_{86} using single crystal X-ray diffraction analysis. Crystallographic analysis shows that, while in most previously reported cluster fullerenes, clusters intend to take a central position inside fullerene cages, in these two structures, the Sc_3N clusters are notably shifted to one side of the cage and unexpectedly pyramidalized, which resembles a spider attached to a web. These observations, together with the stretched Sc–N bonds, suggest that the endohedral M_3N cluster can self-adjust not only its size and configuration, but also its position relative to fullerenes to optimize the metal–cage distances as well as cluster–cage interactions, thus promoting stability with large cages. This work not only validates the stability of endohedral structures with large carbon cages encapsulating small nitride clusters, but also, more importantly, reveals the unexpected flexibility of cluster–cage interactions, which provides new insight into the interaction mechanisms between the metal clusters and carbon cages of EMFs.

Experimental

Synthesis and isolation of $Sc_3N@C_{2n}$ ($2n$ = 84 and 86)

Carbon soot containing scandium NCFs was synthesized by a direct-current arc discharge method. Graphite rods packed with Sc_2O_3 and graphite powder (1.02 g of Sc_2O_3 powder and 1.97 g of graphite powder per rod and a molar ratio of Sc/C = 1 : 15) were vaporized in an arcing chamber under a 200 Torr helium atmosphere with 4 Torr N_2. The collected raw soot was extracted with carbon disulfide (CS_2) for 24 h. The separation and purification of $Sc_3N@C_{2n}$ ($2n$ = 84 and 86) were achieved using multi-stage HPLC procedures. Multiple HPLC columns, including a Buckyprep-M column (25 × 250 mm, Cosmosil, Nacalai Tesque Inc.), a Buckyprep-D column (10 × 250 mm, Cosmosil, Nacalai Tesque, Japan), a 5PBB column (10 × 250 mm, Cosmosil, Nacalai Tesque, Japan), and a Buckprep column (10 × 250 mm, Cosmosil, Nacalai Tesque, Japan), were used in the procedures (further details are described in the ESI†).

Spectroscopic studies

A positive-ion mode matrix-assisted laser desorption ionization time-of-flight (MALDI-TOF) mass spectrometer (Bruker, Germany) was used for mass characterization. The UV–vis–NIR spectra of purified $Sc_3N@C_{2n}$ ($2n$ = 84 and 86) were recorded in CS_2 solution with a Cary 5000 UV–vis–NIR spectrophotometer (Agilent, USA).

X-ray crystallographic study

The black block crystals of $Sc_3N@C_{2n}$ ($2n$ = 84 and 86) were obtained by slow diffusion of the carbon disulfide solution of the corresponding metallofullerene compounds into a benzene solution of [Ni^{II}(OEP)]. The single-crystal X-ray data of $Sc_3N@C_{84}$ and $Sc_3N@C_{86}$ were collected at 120 K on a diffractometer (APEX II; Bruker Analytik GmbH) equipped with a CCD collector. The multiscan method was used for absorption correction. The structures were solved using intrinsic phasing methods[46] and refined on F^2 using full-matrix least-squares with the SHELXL 2018 crystallographic software package.[47] Hydrogen atoms were inserted at calculated positions and constrained with isotropic thermal parameters.

Crystal data for $Sc_3N@C_s(51365)$-C_{84}·[Ni^{II}(OEP)]: M_r = 1749.19, 0.12 mm × 0.1 mm × 0.07 mm, triclinic, $P\bar{1}$ (no. 2), a = 14.6460(18) Å, b = 14.9090(19) Å, c = 19.743(3) Å, α = 85.084(7)°, β = 88.542(7)°, γ = 62.548(7)°, V = 3811.0(9) Å^3, Z = 2, ρ_{calcd} = 1.524 g cm^{-3}, μ(Ga Kα) = 3.152 mm^{-1}, θ = 1.954–52.000, T = 120(2) K, R_1 = 0.1245, and wR_2 = 0.3112 for all data; R_1 = 0.1038 and wR_2 = 0.2927 for 9662 reflections ($I > 2.0\sigma(I)$) with 1199 parameters. The goodness-of-fit indicator was 1.057. The maximum residual electron density was 1.735 e Å^{-3}.

Crystal data for $Sc_3N@D_3(19)$-C_{86}·[Ni^{II}(OEP)]·C_6H_6: M_r = 1851.32, 0.1 mm × 0.08 mm × 0.06 mm, monoclinic, $C2/m$ (no. 12), a = 26.259(3) Å, b = 17.9994(19) Å, c = 17.8301(16) Å, α = 90°, β = 108.472(4)°, γ = 90°, V = 7993.0(14) Å^3, Z = 4, ρ_{calcd} = 1.538 g cm^{-3}, μ(Ga Kα) = 3.028 mm^{-1}, θ = 2.273–53.906, T = 120(2) K, R_1 = 0.1430, and wR_2 = 0.2667 for all data; R_1 = 0.0904 and wR_2 = 0.2305 for 4504 reflections ($I > 2.0\sigma(I)$) with 1244 parameters. The goodness-of-fit indicator was 1.057. The maximum residual electron density was 0.758 e Å^{-3}.

The crystallographic data for these two structures have been deposited at the Cambridge Crystallographic Data Centre (CCDC) with the deposition numbers 2178354 and 2178355.†

Conflicts of interest

There are no conflicts to declare.

Acknowledgements

N. C. thanks the National Science Foundation China (NSFC nos 52172051 and 91961109), the Natural Science Foundation of Jiangsu Province (BK20200041) and the Priority Academic Program Development of Jiangsu Higher Education Institutions (PAPD).

Notes and references

1 X. Lu, L. Feng, T. Akasaka and S. Nagase, Current status and future developments of endohedral metallofullerenes, *Chem. Soc. Rev.*, 2012, **41**, 7723–7760.

2 A. A. Popov, S. Yang and L. Dunsch, Endohedral fullerenes, *Chem. Rev.*, 2013, **113**, 5989–6113.
3 L. Bao, P. Peng and X. Lu, Bonding inside and outside fullerene cages, *Acc. Chem. Res.*, 2018, **51**, 810–815.
4 W. Li, F. Qu, L. Liu, Z. Zhang, J. Liang, Y. Lu, J. Zhang, L. Wang, C. Wang and T. Wang, A metallofullertube of $Ce_2@C_{100}$ with a carbon nanotube segment: synthesis, single-molecule conductance and supramolecular assembly, *Angew. Chem.*, 2022, **61**, e202116854.
5 A. R. Puente Santiago, M. F. Sanad, A. Moreno-Vicente, M. A. Ahsan, M. R. Cerón, Y.-R. Yao, S. T. Sreenivasan, A. Rodriguez-Fortea, J. M. Poblet and L. Echegoyen, A new class of molecular electrocatalysts for hydrogen evolution: Catalytic activity of $M_3N@C_{2n}$ ($2n$ = 68, 78, and 80) fullerenes, *J. Am. Chem. Soc.*, 2021, **143**, 6037–6042.
6 C. Zhou, M. Zhen, M. Yu, X. Li, T. Yu, J. Liu, W. Jia, S. Liu, L. Li, J. Li, Z. Sun, Z. Zhao, X. Wang, X. Zhang, C. Wang and C. Bai, Gadofullerene inhibits the degradation of apolipoprotein B100 and boosts triglyceride transport for reversing hepatic steatosis, *Sci. Adv.*, 2020, **6**, eabc1586.
7 K. Zhang, C. Wang, M. Zhang, Z. Bai, F.-F. Xie, Y.-Z. Tan, Y. Guo, K.-J. Hu, L. Cao, S. Zhang, X. Tu, D. Pan, L. Kang, J. Chen, P. Wu, X. Wang, J. Wang, J. Liu, Y. Song, G. Wang, F. Song, W. Ji, S.-Y. Xie, S.-F. Shi, M. A. Reed and B. Wang, A $Gd@C_{82}$ single-molecule electret, *Nat. Nanotechnol.*, 2020, **15**, 1019–1024.
8 S. Stevenson, G. Rice, T. Glass, K. Harich, F. Cromer, M. R. Jordan, J. Craft, E. Hadju, R. Bible, M. M. Olmstead, K. Maitra, A. J. Fisher, A. L. Balch and H. C. Dorn, Small-bandgap endohedral metallofullerenes in high yield and purity, *Nature*, 1999, **401**, 55–57.
9 S. Yang, T. Wei and F. Jin, When metal clusters meet carbon cages: endohedral clusterfullerenes, *Chem. Soc. Rev.*, 2017, **46**, 5005–5058.
10 Q. Tang, L. Abella, Y. Hao, X. Li, Y. Wan, A. Rodríguez-Fortea, J. M. Poblet, L. Feng and N. Chen, $Sc_2O@C_{2v}(5)$-C_{80}: Dimetallic oxide cluster inside a C_{80} fullerene cage, *Inorg. Chem.*, 2015, **54**, 9845–9852.
11 Q. Tang, L. Abella, Y. Hao, X. Li, Y. Wan, A. Rodríguez-Fortea, J. M. Poblet, L. Feng and N. Chen, $Sc_2O@C_{3v}(8)$-C_{82}: A missing isomer of $Sc_2O@C_{82}$, *Inorg. Chem.*, 2016, **55**, 1926–1933.
12 T. Yang, Y. Hao, L. Abella, Q. Tang, X. Li, Y. Wan, A. Rodríguez-Fortea, J. M. Poblet, L. Feng and N. Chen, $Sc_2O@T_d(19151)$-C_{76}: Hindered cluster motion inside a tetrahedral carbon cage probed by crystallographic and computational studies, *Chem. – Eur. J.*, 2015, **21**, 11110–11117.
13 Q. Deng and A. A. Popov, Clusters encapsulated in endohedral metallofullerenes: How strained are they?, *J. Am. Chem. Soc.*, 2014, **136**, 4257–4264.
14 C.-H. Chen, K. B. Ghiassi, M. R. Cerón, M. A. Guerrero-Ayala, L. Echegoyen, M. M. Olmstead and A. L. Balch, Beyond the butterfly: $Sc_2C_2@C_{2v}(9)$-C_{86}, an endohedral fullerene containing a planar, twisted Sc_2C_2 unit with remarkable crystalline order in an unprecedented carbon cage, *J. Am. Chem. Soc.*, 2015, **137**, 10116–10119.
15 S. Hu, P. Zhao, W. Shen, M. Ehara, Y. Xie, T. Akasaka and X. Lu, Crystallographic characterization of $Er_2C_2@C_{80-88}$: Cluster stretching with cage elongation, *Inorg. Chem.*, 2020, **59**, 1940–1946.
16 F. Liu, C.-L. Gao, Q. Deng, X. Zhu, A. Kostanyan, R. Westerström, S. Wang, Y.-Z. Tan, J. Tao, S.-Y. Xie, A. A. Popov, T. Greber and S. Yang, Triangular monometallic cyanide cluster entrapped in carbon cage with geometry-dependent molecular magnetism, *J. Am. Chem. Soc.*, 2016, **138**, 14764–14771.
17 R. Guan, M. Chen, J. Xin, X.-M. Xie, F. Jin, Q. Zhang, S.-Y. Xie and S. Yang, Capturing the missing carbon cage isomer of C_{84} via mutual stabilization of a triangular monometallic cyanide cluster, *J. Am. Chem. Soc.*, 2021, **143**, 8078–8085.
18 J. Xin, F. Jin, R. Guan, M. Chen, X.-M. Xie, Q. Zhang, S.-Y. Xie and S. Yang, Ancient pigment to treasure: Prussian blue as a cheap solid cyanide/nitrogen dual-source affording the high-yield syntheses of pricey endohedral clusterfullerenes, *Inorg. Chem. Front.*, 2021, **8**, 1719–1726.
19 J. Zhang, T. Fuhrer, W. Fu, J. Ge, D. W. Bearden, J. Dallas, J. Duchamp, K. Walker, H. Champion, H. Azurmendi, K. Harich and H. C. Dorn, Nanoscale fullerene compression of an yttrium carbide cluster, *J. Am. Chem. Soc.*, 2012, **134**, 8487–8493.
20 W. Shen, Z. Hu, P. Yu, Z. Wei, P. Jin, Z. Shi and X. Lu, An experimental and theoretical study of $LuNC@C_{76,82}$ revealing a cage-cluster selection rule, *Inorg. Chem. Front.*, 2020, **7**, 4563–4571.
21 H. W. Kroto, The stability of the fullerenes C_n, with n = 24, 28, 32, 36, 50, 60 and 70, *Nature*, 1987, **329**, 529–531.
22 Y. Zhang, K. B. Ghiassi, Q. Deng, N. A. Samoylova, M. M. Olmstead, A. L. Balch and A. A. Popov, Synthesis and structure of $LaSc_2N@C_s$(hept)-C_{80} with one heptagon and thirteen pentagons, *Angew. Chem., Int. Ed.*, 2015, **54**, 495–499.
23 C.-H. Chen, L. Abella, M. R. Cerón, M. A. Guerrero-Ayala, A. Rodríguez-Fortea, M. M. Olmstead, X. B. Powers, A. L. Balch, J. M. Poblet and L. Echegoyen, Zigzag Sc_2C_2 carbide cluster inside a [88]fullerene cage with one heptagon, $Sc_2C_2@C_s$(hept)-C_{88}: A kinetically trapped fullerene formed by C_2 insertion?, *J. Am. Chem. Soc.*, 2016, **138**, 13030–13037.
24 C. M. Beavers, M. N. Chaur, M. M. Olmstead, L. Echegoyen and A. L. Balch, Large metal ions in a relatively small fullerene cage: The structure of $Gd_3N@C_2(22010)$-C_{78} departs from the isolated pentagon rule, *J. Am. Chem. Soc.*, 2009, **131**, 11519–11524.
25 S. Stevenson, A. J. Rothgeb, K. R. Tepper, J. Duchamp, H. C. Dorn, X. B. Powers, M. Roy, M. M. Olmstead and A. L. Balch, Isolation and crystallographic characterization of two, nonisolated pentagon endohedral fullerenes: $Ho_3N@C_2(22010)$-C_{78} and $Tb_3N@C_2(22010)$-C_{78}, *Chem. – Eur. J.*, 2019, **25**, 12545–12551.
26 B. Q. Mercado, C. M. Beavers, M. M. Olmstead, M. N. Chaur, K. Walker, B. C. Holloway, L. Echegoyen and

A. L. Balch, Is the isolated pentagon rule merely a suggestion for endohedral fullerenes? The structure of a second egg-shaped endohedral fullerene—$Gd_3N@C_s$(39663)-C_{82}, *J. Am. Chem. Soc.*, 2008, **130**, 7854–7855.

27 M. Guo, X. Li, Y.-R. Yao, J. Zhuang, Q. Meng, Y. Yan, X. Liu and N. Chen, A non-isolated pentagon rule C_{82} cage stabilized by a stretched Sc_3N cluster, *Chem. Commun.*, 2021, **57**, 4150–4153.

28 X. Aparicio-Anglès, N. Alegret, A. Clotet, A. Rodríguez-Fortea and J. M. Poblet, Endohedral metallofullerenes containing lanthanides: A robust yet simple computational approach, *J. Phys. Chem. C*, 2013, **117**, 12916–12921.

29 S. Stevenson, J. P. Phillips, J. E. Reid, M. M. Olmstead, S. P. Rath and A. L. Balch, Pyramidalization of Gd_3N inside a C_{80} cage. The synthesis and structure of $Gd_3N@C_{80}$, *Chem. Commun.*, 2004, 2814–2815, DOI: 10.1039/B412338G.

30 L. Echegoyen, C. J. Chancellor, C. M. Cardona, B. Elliott, J. Rivera, M. M. Olmstead and A. L. Balch, X-Ray crystallographic and EPR spectroscopic characterization of a pyrrolidine adduct of $Y_3N@C_{80}$, *Chem. Commun.*, 2006, 2653–2655, DOI: 10.1039/B604011J.

31 T. Zuo, C. M. Beavers, J. C. Duchamp, A. Campbell, H. C. Dorn, M. M. Olmstead and A. L. Balch, Isolation and structural characterization of a family of endohedral fullerenes including the large, chiral cage fullerenes $Tb_3N@C_{88}$ and $Tb_3N@C_{86}$ as well as the I_h and D_{5h} isomers of $Tb_3N@C_{80}$, *J. Am. Chem. Soc.*, 2007, **129**, 2035–2043.

32 A. A. Popov and L. Dunsch, Structure, stability, and cluster-cage interactions in nitride clusterfullerenes $M_3N@C_{2n}$ (M = Sc, Y; $2n$ = 68–98): A density functional theory study, *J. Am. Chem. Soc.*, 2007, **129**, 11835–11849.

33 C. M. Beavers, T. Zuo, J. C. Duchamp, K. Harich, H. C. Dorn, M. M. Olmstead and A. L. Balch, $Tb_3N@C_{84}$: An improbable, egg-shaped endohedral fullerene that violates the isolated pentagon rule, *J. Am. Chem. Soc.*, 2006, **128**, 11352–11353.

34 T. Zuo, K. Walker, M. M. Olmstead, F. Melin, B. C. Holloway, L. Echegoyen, H. C. Dorn, M. N. Chaur, C. J. Chancellor, C. M. Beavers, A. L. Balch and A. J. Athans, New egg-shaped fullerenes: Non-isolated pentagon structures of $Tm_3N@C_s$(51365)-C_{84} and $Gd_3N@C_s$(51365)-C_{84}, *Chem. Commun.*, 2008, 1067–1069, DOI: 10.1039/B716037B.

35 W.-Q. Shen, L.-P. Bao, S.-F. Hu, X.-J. Gao, Y.-P. Xie, X.-F. Gao, W.-H. Huang and X. Lu, Isolation and crystallographic characterization of $Lu_3N@C_{2n}$ ($2n$ = 80–88): Cage selection by cluster size, *Chem. – Eur. J.*, 2018, **24**, 16692–16698.

36 S. Hu, P. Zhao, W. Shen, P. Yu, W. Huang, M. Ehara, Y. Xie, T. Akasaka and X. Lu, Crystallographic characterization of $Er_3N@C_{2n}$ ($2n$ = 80, 82, 84, 88): The importance of a planar Er_3N cluster, *Nanoscale*, 2019, **11**, 13415–13422.

37 M. N. Chaur, X. Aparicio-Anglès, B. Q. Mercado, B. Elliott, A. Rodríguez-Fortea, A. Clotet, M. M. Olmstead, A. L. Balch, J. M. Poblet and L. Echegoyen, Structural and electrochemical property correlations of metallic nitride endohedral metallofullerenes, *J. Phys. Chem. C*, 2010, **114**, 13003–13009.

38 S. Stevenson, P. W. Fowler, T. Heine, J. C. Duchamp, G. Rice, T. Glass, K. Harich, E. Hajdu, R. Bible and H. C. Dorn, A stable non-classical metallofullerene family, *Nature*, 2000, **408**, 427–428.

39 M. M. Olmstead, H. M. Lee, J. C. Duchamp, S. Stevenson, D. Marciu, H. C. Dorn and A. L. Balch, $Sc_3N@C_{68}$: Folded pentalene coordination in an endohedral fullerene that does not obey the isolated pentagon rule, *Angew. Chem., Int. Ed.*, 2003, **42**, 900–903.

40 T. Cai, L. Xu, M. R. Anderson, Z. Ge, T. Zuo, X. Wang, M. M. Olmstead, A. L. Balch, H. W. Gibson and H. C. Dorn, Structure and enhanced reactivity rates of the D_{5h} $Sc_3N@C_{80}$ and $Lu_3N@C_{80}$ metallofullerene isomers: The importance of the pyracylene motif, *J. Am. Chem. Soc.*, 2006, **128**, 8581–8589.

41 T. Wei, S. Wang, F. Liu, Y. Tan, X. Zhu, S. Xie and S. Yang, Capturing the long-sought small-bandgap endohedral fullerene $Sc_3N@C_{82}$ with low kinetic stability, *J. Am. Chem. Soc.*, 2015, **137**, 3119–3123.

42 M. M. Olmstead, A. de Bettencourt-Dias, J. C. Duchamp, S. Stevenson, D. Marciu, H. C. Dorn and A. L. Balch, Isolation and structural characterization of the endohedral fullerene $Sc_3N@C_{78}$, *Angew. Chem., Int. Ed.*, 2001, **40**, 1223–1225.

43 S. Yang, A. A. Popov and L. Dunsch, Violating the isolated pentagon rule (IPR): The endohedral non-IPR C_{70} cage of $Sc_3N@C_{70}$, *Angew. Chem., Int. Ed.*, 2007, **46**, 1256–1259.

44 M. N. Chaur, F. Melin, B. Elliott, A. Kumbhar, A. J. Athans and L. Echegoyen, New $M_3N@C_{2n}$ endohedral metallofullerene families (M = Nd, Pr, Ce; n = 40–53): Expanding the preferential templating of the C_{88} cage and approaching the C_{96} cage, *Chem. – Eur. J.*, 2008, **14**, 4594–4599.

45 M. N. Chaur, R. Valencia, A. Rodríguez-Fortea, J. M. Poblet and L. Echegoyen, Trimetallic nitride endohedral fullerenes: Experimental and theoretical evidence for the $M_3N^{6+}@C_{2n}^{6-}$ model, *Angew. Chem., Int. Ed.*, 2009, **48**, 1425–1428.

46 O. V. Dolomanov, L. J. Bourhis, R. J. Gildea, J. A. K. Howard and H. Puschmann, $OLEX_2$: A complete structure solution, refinement and analysis program, *J. Appl. Crystallogr.*, 2009, **42**, 339–341.

47 G. Sheldrick, Crystal structure refinement with SHELXL, *Acta Crystallogr., Sect. C: Struct. Chem.*, 2015, **71**, 3–8.

